


# Connecting relaxation time to a dynamical length scale in athermal active glass formers

Dipanwita Ghoshal  and Ashwin Joy\*

*Department of Physics, Indian Institute of Technology Madras, Chennai, Tamil Nadu 600036, India*

 (Received 12 August 2020; revised 21 October 2020; accepted 17 November 2020; published 7 December 2020)

Supercooled liquids display dynamics that are inherently heterogeneous in space. This essentially means that at temperatures below the melting point, particle dynamics in certain regions of the liquid can be orders of magnitude faster than other regions. Often dubbed dynamical heterogeneity, this behavior has fascinated researchers involved in the study of glass transition for over two decades. A fundamentally important question in all glass transition studies is whether one can connect the growing relaxation time to a concomitantly growing length scale. In this paper, we go beyond the realm of ordinary glass forming liquids and study the origin of a growing dynamical length scale  $\xi$  in a self-propelled “active” glass former. This length scale, which is constructed using structural correlations, agrees well with the average size of the clusters of slow-moving particles that are formed as the liquid becomes spatially heterogeneous. We further report that the concomitantly growing  $\alpha$ -relaxation time exhibits a simple scaling law,  $\tau_\alpha \sim \exp(\mu\xi/T_{\text{eff}})$ , with  $\mu$  as an effective chemical potential,  $T_{\text{eff}}$  as the effective temperature, and  $\mu\xi$  as the growing free energy barrier for cluster rearrangements. The findings of our study are valid over four decades of persistence times, and hence they could be very useful in understanding the slow dynamics of a generic active liquid such as an active colloidal suspension, or a self-propelled granular medium.

DOI: [10.1103/PhysRevE.102.062605](https://doi.org/10.1103/PhysRevE.102.062605)

## I. INTRODUCTION

It is well known that liquids near a glass transition display a growing length scale [1–5] that is normally associated with the concomitant sluggish dynamics. This growing length scale in a typical glass former often characterizes the spatial extent of dynamic heterogeneity, and the literature on this subject is quite extensive [2,6,7]. The aforementioned heterogeneity in space and time is ubiquitous in nature and also observed in active systems having an internal source of energy, ranging from biological cells [8] and tissues [9] to even ant colonies [10]. The visual identification of dynamic heterogeneity in a glass forming liquid at low temperatures often requires a definition of a cluster of particles moving slower than the surrounding medium. The average size of these clusters, which can be treated as a growing length scale, tends to increase as one approaches the glass transition, and the cooperative movement of these large clusters results in the observed sluggish dynamics. There exist numerous reports on the study of growing length scales in passive glass forming liquids, covering extensive simulations [3–5,11–14], experiments [15–17], and theoretical investigations [18–22]. However, similar explorations of a growing length scale in active glass formers remain limited in scope. Here we study the dynamic heterogeneity in a system of self-propelled particles, and we explore various growing length scales that are concomitant with sluggish dynamics near the glass transition. The active liquid in our study is represented by a minimal Ornstein-Uhlenbeck (OU) model in which the activity is

completely described by only two parameters, the persistence time  $\tau_p$  and the effective temperature  $T_{\text{eff}}$ . The model can be used to study active colloidal suspensions, passive tracers in bacterial baths, and self-propelled granular media, to mention a few. In what follows, we provide a brief background covering some results that are relevant to our study.

It is well established that the four-point structure factor is maximum around the  $\alpha$ -relaxation time ( $\tau_\alpha$ ) for typical glass forming systems [4,5], and it can be profitably used to extract a dynamical length scale ( $\xi$ ). In this paper, we have extracted  $\xi$  and two other length scales, namely the microscopic hexatic length scale  $\xi_6$  and the diffusion length scale  $\sqrt{D\tau_\alpha}$ . We also find that at lower temperatures, the dynamical length scale  $\xi$  decouples from all the other length scales examined here—an observation made earlier in some works on passive glass formers [23–25]. The dynamic length scale  $\xi$  extracted from long-range structural correlations can be connected to the concomitant growing  $\alpha$ -relaxation time scale  $\tau_\alpha$  through a simple scaling law,  $\tau_\alpha \sim \exp(\mu\xi/T_{\text{eff}})$ , that is similar to predictions from the random first-order transition theory (RFOT) [26,27] in two dimensions. Our results are valid over four decades of persistence time, and at every  $\tau_p, T_{\text{eff}}$  state point the size of the slow-moving clusters agrees well with the dynamic length scale  $\xi$ . We conclude the paper with the role of persistence time  $\tau_p$  on the chemical potential  $\mu$ , which is essentially an energy cost per unit length to form clusters of slow-moving particles.

The paper is organized into the following sections. Section I discusses the introduction and necessary background of the subject, Sec. II presents the minimal model used in our work to describe an athermal active glass forming liquid, Sec. III presents a discussion of our results, and finally in

\*ashwin@physics.iitm.ac.in

Sec. IV we summarize our work and present interesting future directions resulting from our work. We will now discuss the numerical model used in our work.

## II. MINIMAL MODEL

There is enough evidence to suggest that fluids composed of active particles can exhibit glassy dynamics at sufficiently high particulate densities, notable mentions being experiments on migrating cells [8] and embryonic tissues [9], as well as numerical simulations [28]. There have been some recent reports on the influence of activity on the sluggish dynamics in glass forming systems [28–32], but the results depend qualitatively on the presence of thermal noise in the system. In our work, we use an athermal model of self-propelled particles introduced earlier [28,33–35]. The model is deemed athermal as there is no explicit presence of thermal noise term in the position update of the particles. The governing equations for the  $i$ th particle with mass  $m$  read

$$\begin{aligned}\dot{\mathbf{r}}_i &= \frac{1}{m\gamma} \left[ -\sum_{j \neq i} \nabla_i \phi(r_{ij}) + \mathbf{f}_i \right], \\ \dot{\mathbf{f}}_i &= \frac{1}{\tau_p} \left[ -\mathbf{f}_i + \sqrt{2m\gamma k_B T_{\text{eff}}} \boldsymbol{\eta}_i \right].\end{aligned}\quad (1)$$

$$\phi(r_{ij}) = \begin{cases} 4\epsilon_{ij} \left[ \left( \frac{\sigma_{ij}}{r_{ij}} \right)^{12} - \left( \frac{\sigma_{ij}}{r_{ij}} \right)^6 \right], & 0 < r_{ij} \leq r_m, \\ \epsilon_{ij} \left[ A \left( \frac{\sigma_{ij}}{r_{ij}} \right)^{12} - \left( \frac{\sigma_{ij}}{r_{ij}} \right)^6 + \sum_{p=0}^3 C_{2p} \left( \frac{r_{ij}}{\sigma_{ij}} \right)^p \right], & r_m < r_{ij} \leq r_c, \\ 0, & r > r_c, \end{cases}\quad (4)$$

that is smoothly truncated to zero along with its first two derivatives, at the cutoff distance  $r_c$ . The parameters  $A$ ,  $B$ ,  $C_0$ ,  $C_2$ ,  $C_4$ , and  $C_6$  are obtained by matching  $\phi$  and its two derivatives at the boundaries  $r_m$  and  $r_c$ . We have employed the celebrated Kob-Andersen (KA) [36,37] binary glass former where the ratio of large ( $L$ ) to small ( $S$ ) particles is kept as 80:20. All particles have the same mass  $m$  irrespective of their size. We took  $\epsilon_{\text{LL}}$ ,  $\sigma_{\text{LL}}$ , and  $\sqrt{m\sigma_{\text{LL}}^2/\epsilon_{\text{LL}}}$  as the characteristic units of energy, length, and time, respectively. In these units, the potential parameters become  $\epsilon_{\text{SS}} = 0.5$ ,  $\epsilon_{\text{LS}} = 1.5$ ,  $\sigma_{\text{SS}} = 0.88$ , and  $\sigma_{\text{LS}} = 0.80$ . The inner and outer cutoff distances are then, respectively,  $r_m = 1.12246$  and  $r_c = 2.5$ . The density is fixed at  $\rho = 1.20$  throughout our paper. It should be noted that a finite temperature divergence of the relaxation time in the three-dimensional equilibrium KA liquid is known to happen at the mode coupling temperature  $T_c = 0.435$ , which also serves as the upper bound for the glass transition temperature  $T_g$ . A similar finite temperature divergence is not expected in equilibrium 2D liquids due to the presence of Mermin-Wagner-like fluctuations [38,39] that tend to grow logarithmically with the system size and eliminate any transient localization of particles that is necessary for a plateau to develop in the self-intermediate scattering function [40–42]. Since our primary objective was to extract a growing length scale through long-wavelength structural correlations, we have employed a 2D periodic box with  $N = 10\,000$

Put simply, the dynamics is overdamped with  $m\gamma$  as the friction coefficient and falls under the Ornstein-Uhlenbeck (OU) type of stochastic process that has been used to model athermal active systems. The self-propulsion force  $\mathbf{f}_i$  is a colored noise with an exponentially decaying autocorrelation function given by

$$\langle f_{i\alpha}(t) f_{j\beta}(t') \rangle_{\text{noise}} = \left( \frac{m\gamma k_B T_{\text{eff}}}{\tau_p} \right) \delta_{\alpha\beta} \delta_{ij} e^{-|t-t'|/\tau_p}, \quad (2)$$

where the Greek symbols  $\alpha$ ,  $\beta$  and the Latin symbols  $i$ ,  $j$  denote, respectively, the vector components and particle labels. We take  $\boldsymbol{\eta}_i$  to be a Gaussian white noise of zero mean and unit variance,

$$\langle \eta_{i\alpha}(t) \eta_{j\beta}(t') \rangle_{\text{noise}} = \delta_{\alpha\beta} \delta_{ij} \delta(t - t'). \quad (3)$$

The angular brackets  $\langle \dots \rangle_{\text{noise}}$  refer to an average in the distribution of noise under consideration. The particles interact through the Lennard-Jones potential,

particles that conforms to a square box of size  $L = 91.2871$ , and is large enough for our work. To integrate Eq. (1), we used a stochastic velocity Verlet algorithm [43] with a time step of  $\Delta t = 0.0001$  that guaranteed numerical stability in the entire parameter range explored in this paper. To assert the robustness of our results, we performed our study over a wide range of persistence times  $\tau_p$ , ranging from 0.0002, which corresponds to the limit of equilibrium Brownian dynamics (BD), to all the way up to 1.0, which is far from equilibrium. We explore effective temperatures in the range  $0.35 \leq T_{\text{eff}} \leq 2.50$ , where the former limit corresponds to a strongly supercooled regime with significant cooperative dynamics, and the latter corresponding to a high-temperature limit where cooperative behavior is absent. Below, we discuss our results in detail.

## III. RESULTS AND DISCUSSION

### A. Dynamic length scale ( $\xi$ )

To extract the dynamic length scale  $\xi$ , we evaluate the four-point structure factor [44,45]

$$S_4(\mathbf{q}; \tau) = \frac{1}{N} (\langle Q(\mathbf{q}; \tau) Q(-\mathbf{q}; \tau) \rangle - |\langle Q(\mathbf{q}; \tau) \rangle|^2), \quad (5)$$

where  $\mathbf{q}$  is a typical wave vector and  $\tau$  is an elapsed time interval. The angular brackets used here denote an ensemble average over 100 independent realizations of the system

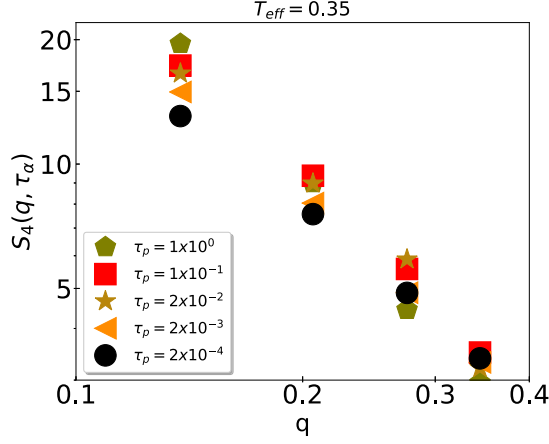


FIG. 1. Four-point structure factor as a function of wave vector at a typical low temperature. The long-wavelength ( $q \rightarrow 0$ ) collective behavior is amplified by increasing the persistence time  $\tau_p$ . One can therefore expect the formation of larger clusters with increasing  $\tau_p$  at any given effective temperature; see Fig. 4.

and two independent wave vectors for a given magnitude, namely  $\{(0, q), (q, 0)\}$ . We define  $Q(\mathbf{q}; \tau)$  as the Fourier transform

$$Q(\mathbf{q}; \tau) = \sum_{n=1}^N w_n(\tau) \exp[-i\mathbf{q} \cdot \mathbf{r}_n(0)] \quad (6)$$

of the filtered-particle density

$$Q(\mathbf{r}; \tau) = \sum_{m=1}^N w_m(\tau) \delta(\mathbf{r} - \mathbf{r}_m(0)),$$

where the summations run over all particles in the system. To calculate the quantities mentioned above, we have used a microscopic overlap function defined as

$$w_n(\tau) = \Theta[a - |\mathbf{r}_n(\tau) - \mathbf{r}_n(0)|]. \quad (7)$$

Here  $\Theta(x)$  is the Heaviside step function that serves to filter out the particles that do not move farther than a specified distance  $a$ , during the time interval  $\tau$ . We have taken  $a = 0.3$ , which roughly corresponds to the plateau value of the mean-squared displacement (MSD) at all temperatures. Denoting the  $\alpha$ -relaxation time,  $\tau_\alpha$ , to be the time at which the self-intermediate scattering function falls  $1/e$  of its initial value, we plot our data on  $S_4(q; \tau_\alpha)$  at a typical low effective temperature in Fig. 1. It is evident from the figure that at any given effective temperature, the long-wavelength ( $q \rightarrow 0$ ) response increases with the persistence time  $\tau_p$ , suggesting to us that the dynamical length scale  $\xi$  must increase with the persistence time  $\tau_p$ . To extract  $\xi$  at any fixed pair of  $(\tau_p, T_{\text{eff}})$ , we fit our  $S_4(q; \tau_\alpha)$  data to the following Ornstein-Zernike (OZ) relationship:

$$S_4(q; \tau_\alpha) = \frac{A}{1 + (q\xi)^2}, \quad (8)$$

where  $A = \lim_{q \rightarrow 0} S_4(q; \tau_\alpha)$  and  $\xi$  are fitting parameters for the chosen  $(\tau_p, T_{\text{eff}})$  pair; see Fig. 2. The extracted dynamical length scale  $\xi$  is plotted in Fig. 3, where it is evident that at all temperatures, the effect of  $\tau_p$  is to increase the length scale  $\xi$ .

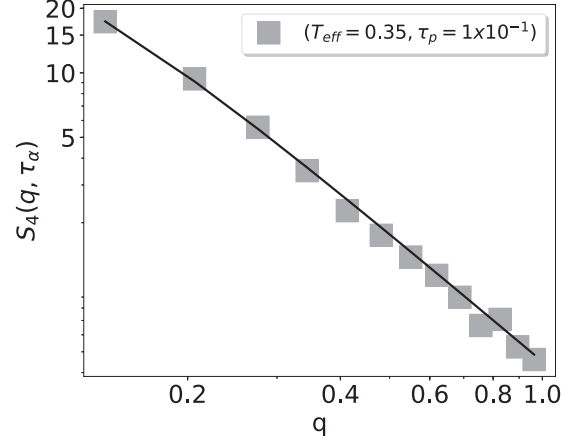


FIG. 2. Our data on  $S_4(q, \tau_\alpha)$  for a typical  $(\tau_p, T_{\text{eff}})$  pair. The solid line is a fit to the OZ relationship mentioned in Eq. (8), and the extracted dynamical length scale  $\xi$  is plotted in Fig. 3.

This explains the formation of larger clusters of slow-moving particles as  $\tau_p$  is lifted at any given  $T_{\text{eff}}$ ; see Fig. 4, where we show the displacement maps of the full system. The reader can easily verify that at any given state point, the size of a typical slow-moving cluster agrees well with our estimated  $\xi$  representing the diameter of the white circles plotted merely to aid the eye of the reader.

The method used here relies on the interplay between dynamics and structure near the glass transition. There are, however, alternative approaches in the context of passive liquids, most notably through inherent structures that are essentially the minima in the rugged potential energy landscape of glass forming liquids [46–50]. We believe that our approach is simpler and has the potential to yield a deep insight into the sluggish dynamics of active glass formers, through the concept of a chemical potential  $\mu$  (described later) that depends on the persistence time  $\tau_p$ . In what follows, we will show that an increase in the persistence time leads to a larger free-energy

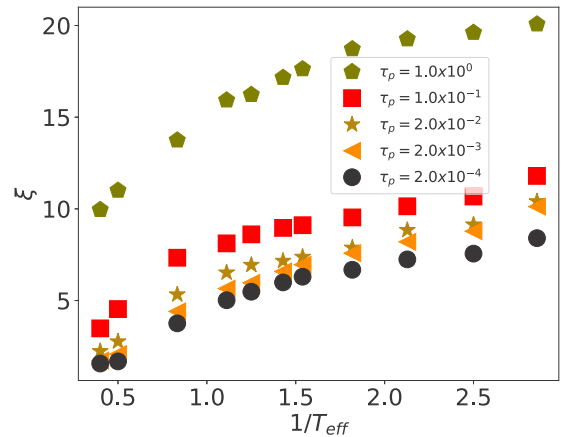


FIG. 3. At any effective temperature, the length scale  $\xi$  increases with the persistence time  $\tau_p$ , and therefore it results in a higher degree of spatial heterogeneity. This behavior manifests in the emergence of larger clusters of slow-moving particles at higher values of persistence times at any specific effective temperature; see Fig. 4.

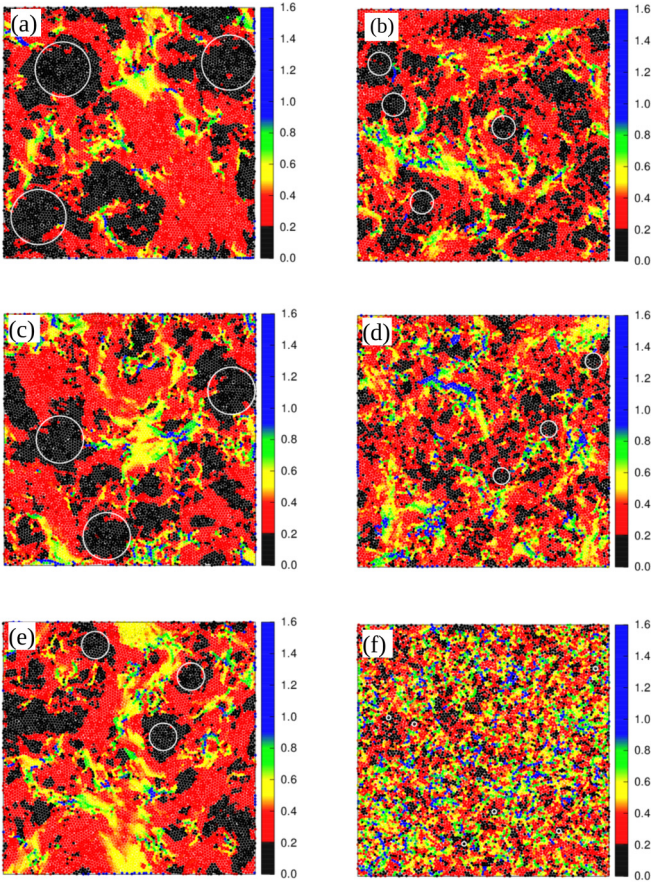


FIG. 4. Snapshots of dynamical clusters for various  $[T_{\text{eff}}, \tau_p]$  pairs, namely (a)  $[0.35, 1.0]$ , (b)  $[0.35, 0.0002]$ , (c)  $[0.70, 1.0]$ , (d)  $[0.70, 0.0002]$ , (e)  $[2.50, 1.0]$ , and (f)  $[2.50, 0.0002]$ . The color bar indicates the magnitude of particle displacements recorded over a specified time, which is set to be of the order of  $\tau_\alpha$ . To aid the eye of the reader, we plot white circles of diameter  $\xi$  extracted from the OZ relation over these slow-moving regions. It is immediately evident that the spatial extent (size) of a typical cluster is in good agreement with our estimate of  $\xi$ . It should be noted that the ratio of  $L$ - to  $S$ -type particles inside these slow-moving clusters remains at the global ratio 80:20 throughout the parameter range explored in our work, thereby ruling out any phase separation dynamics.

barrier for cluster rearrangements, directly leading to the concomitantly growing time scale  $\tau_\alpha$ . It is evident from Fig. 4 that at higher effective temperatures  $T_{\text{eff}}$  and lower persistence times  $\tau_p$ , the system becomes increasingly homogeneous with the cluster size becoming much smaller. On the other hand, decreasing either  $T_{\text{eff}}$  or increasing  $\tau_p$  leads to an increase in cluster size, and therefore spatial heterogeneity. The largest clusters in our study appear in the state  $T_{\text{eff}} = 0.35$  and  $\tau_p = 1 \times 10^0$ . Below we present a simple scaling relationship that connects this growing length scale  $\xi$  to the concomitantly growing time scale  $\tau_\alpha$  that remains valid over a wide range of persistence times.

### B. Free-energy barrier for cluster rearrangements

If we consider  $\mu$  as a chemical potential that needs to be scaled for the formation of a cluster of a certain size  $\xi$ , then

we may assume a simple scaling formula for the relaxation (rearrangement) time of these clusters,

$$\tau_\alpha = \tau_{\alpha 0} \exp \left[ \frac{\mu \xi}{k_B T_{\text{eff}}} \right], \quad (9)$$

where  $\mu$  and  $\tau_{\alpha 0}$  are treated as fitting parameters at any fixed  $\tau_p$ . The product  $\mu \xi$  then refers to the growing free-energy barrier of cluster rearrangements as the effective temperature is lowered, at any fixed  $\tau_p$ . The form of our scaling law is similar to the two-dimensional limit of the random first-order transition theory (RFOT) [26,27] that is known to connect the relaxation time scale to a growing mosaic length scale, with the latter governing the free-energy barriers between the metastable states. Since then, there have been some interesting works on three-dimensional passive glass forming liquids that reported similar scaling laws to connect the relaxation times to an appropriate growing length scale [51]. It should be noted that within RFOT, the dependence of this free-energy barrier on length scale is normally assumed to be a power law with an exponent that is usually unknown, and is only heuristically proposed to be  $d/2$ , with  $d$  as the number of spatial dimensions. Thus in the marginal case of two dimensions, we arrive at  $\Delta F = \mu \xi$ , and it is quite remarkable that our scaling law is able to account for the relaxation times in the active glassy liquid up to four decades of persistence time  $\tau_p$ , all the way up to  $\tau_p = 1.0$ , where the liquid is substantially active. Recently, Nandi *et al.* extended RFOT in active liquids by capturing the modulation of configurational entropy by activity to predict the relaxation time scales in the active liquids [52]. Our work, however, goes a step further and connects the dynamical length scale to the growing relaxation times by computing the cost of cluster rearrangements, namely the free-energy barrier  $\mu \xi$ . Through this picture, we are able to collapse our relaxation time data using just two fitting parameters, namely  $\mu$  and  $\tau_{\alpha 0}$ . Our work has therefore great utility in experiments targeting dynamical heterogeneity in such systems. In Fig. 5, we show both our raw data and a collapse to the scaling law reported in Eq. (9), over four orders of magnitude of the persistence time. The dashed envelope holding identical data points clearly shows that we have collapsed  $\tau_\alpha$  data close to three orders of magnitude. It is indeed remarkable that this simple scaling law remains valid even up to moderate levels of activity where the liquid is far from equilibrium. The quality of the collapse is evident from this figure, particularly at lower effective temperatures, and all the way to the lowest effective temperature accessible in our simulations. It should be noticed that our scaling law predicts a divergence of the relaxation time only as  $T_{\text{eff}} \rightarrow 0$ . The overestimation by our scaling law at high temperatures ( $T_{\text{eff}} > 1.5$ ) can be attributed to the lack of well-defined clusters in this regime as particles do not move cooperatively at these effective temperatures. The high-temperature limit,  $\tau_\alpha / \tau_{\alpha 0} \rightarrow 1$  ( $T_{\text{eff}} \rightarrow \infty$ ), nevertheless is consistent with the expectations from a viable scaling theory.

To understand the effects of the persistence time  $\tau_p$  on the chemical potential  $\mu$ , we provide a table of our fitting parameters (Table I). It is evident from this table that increasing the persistence time leads to a reduction in  $\mu$ , which in turn facilitates the formation of large clusters; see Fig. 4. We propose that  $\mu$  should be realized as the energy cost per unit

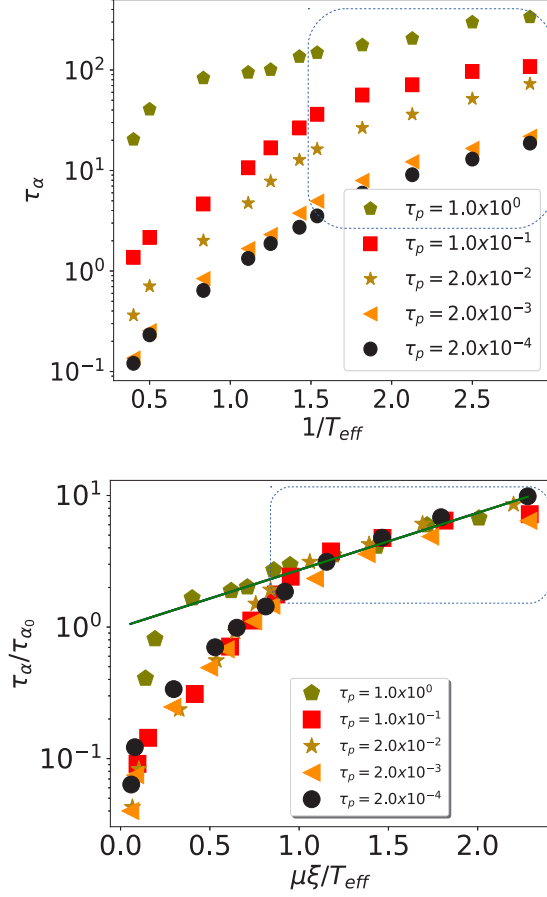


FIG. 5. Top: Unnormalized data show a  $\sim 10^3$  order of magnitude variation of  $\tau_\alpha$ . Bottom: Demonstration of data collapse for the scaled time  $\tau_\alpha/\tau_{\alpha 0}$  vs scaled free energy  $\mu\xi/T_{eff}$  achieved over four decades of  $\tau_p$ . The solid line is a fit to the scaling law in Eq. (9). The dashed envelope in both parts of the figure holds the same data points. Note that the relaxation time is predicted to have a true divergence only at  $T_{eff} \rightarrow 0$ . At very high temperatures, well-defined clusters do not exist, and the scaling law overestimates the relaxation times.

length to form a cluster at any effective temperature, and a lower  $\mu$  therefore implies the formation of bigger clusters. Once clusters of a certain size  $\xi$  are formed, their relaxation times are correctly captured by a free-energy barrier  $\mu\xi$  that is seen to grow with  $1/T_{eff}$  at any given  $\tau_p$ ; see Fig. 6. The effect of persistence time has been beautifully captured by the energy barrier of cluster rearrangements. In what follows, we

TABLE I. Extracted values of  $\tau_{\alpha 0}$  and  $\mu$  for  $\xi$  as fitting parameters. It is evident from Fig. 4 that increasing the persistence time lowers the chemical potential, thereby facilitating the formation of large clusters of slow moving particles; see Fig. 4.

$\tau_p$	$\tau_{\alpha 0}$	$\mu$
1.0	50.0	0.035
0.1	15.0	0.068
0.02	8.5	0.074
0.002	3.0	0.079
0.0002	1.9	0.095

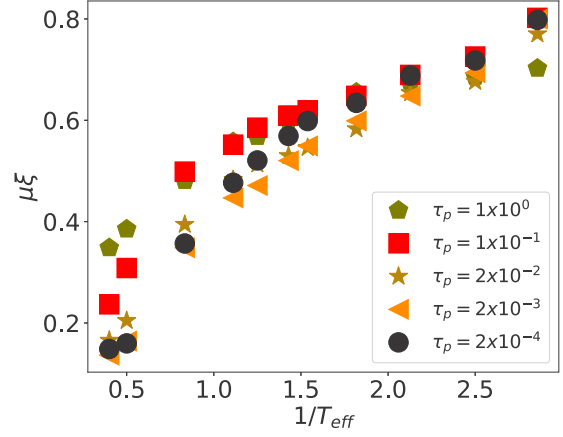


FIG. 6. Growing energy barrier  $\mu\xi$  for cluster rearrangements as a function of effective temperature  $T_{eff}$ . The collapse is evident as  $T_{eff} \rightarrow 0$ , indicating the validity of the scaling law mentioned in Eq. (9).

shall explore some other relevant microscopic length scales in the active liquid that can be constructed from the underlying structure and particle dynamics.

### C. Hexatic length scale ( $\xi_6$ )

The hexatic length scale  $\xi_6$  is a well known static length scale that has been used to study medium range crystalline order (MRCO) in 2D passive glass forming liquids [23,25,53,54]. It is routinely obtained from the spatial correlation function of the hexatic order parameter,

$$\Psi_6 = \left\langle \frac{1}{N} \sum_{j=1}^N \psi_6^j \right\rangle, \quad (10)$$

$$\text{where } \psi_6^j = \frac{1}{n_j} \sum_{k=1}^{n_j} \exp(i6\theta_{jk}), \quad (11)$$

and  $\theta_{jk}$  is the angle between the separation vector  $\mathbf{r}_{jk}$  and a reference axis, say the  $\hat{x}$  axis. Here  $n_j$  refers to the number of Voronoi (nearest) neighbors of any particle  $j$  in the liquid, and  $\langle \dots \rangle$  describes the ensemble average over statistically independent snapshots taken in the steady state. By mathematical construction,  $\psi_6^j$  can range anywhere in the interval  $[0, 1]$  with the values 0 and 1 corresponding, respectively, to a locally disordered and a locally ordered configuration. In Fig. 7, we show instantaneous snapshots of our local order parameter  $\psi_6^j$  to visualize the presence of ordered and disordered regions in our system. It is evident from the figure that the degree of local bond orientation ordering tends to increase only marginally with the persistence time, indicating that the hexatic length scale may not be the dominant length scale that signifies sluggish dynamics. To quantitatively extract a hexatic length scale  $\xi_6$ , we first compute the radial distribution function

$$g(r) = \frac{1}{2\pi r \Delta r \rho(N-1)} \sum_{j \neq k} \delta(r - |\mathbf{r}_{jk}|) \quad (12)$$

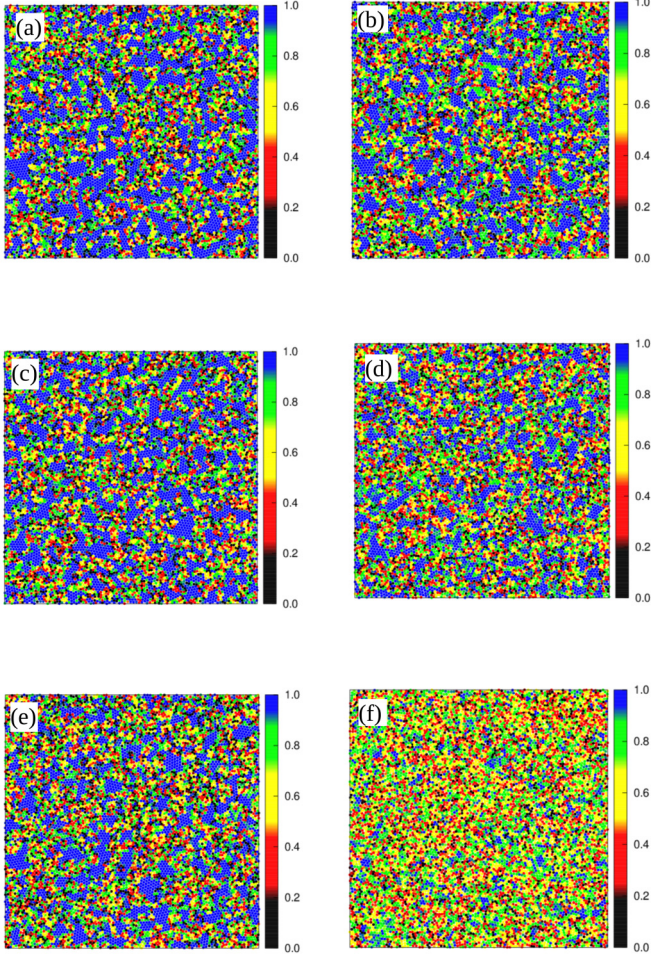


FIG. 7. Color maps of the local bond orientation order parameter  $\psi_6^j$ , where  $j$  is any particle in the system. The panels represent the full system at various  $[T_{\text{eff}}, \tau_p]$  pairs, namely (a)  $[0.35, 0.1]$ , (b)  $[0.35, 0.0002]$ , (c)  $[0.70, 0.1]$ , (d)  $[0.70, 0.0002]$ , (e)  $[2.50, 0.1]$ , and (f)  $[2.50, 0.0002]$ . At lower effective temperatures, increasing the persistence time brings only a marginal increase in the local bond order.

and the spatial correlation of the hexatic order parameter,

$$g_6(r) = \frac{L^2}{2\pi r \Delta r N(N-1)} \sum_{j \neq k} \delta(r - |\mathbf{r}_{jk}|) \psi_6^j \psi_6^{k*}, \quad (13)$$

where the interval  $\Delta r$  is the thickness of a typical annular shell around any particle that has an average number density,  $\rho g(r)$ . In our simulations, we set  $\Delta r = 0.05$ . A numerical fit of the peak values of  $g_6(r)/g(r)$  data to the Ornstein-Zernike (OZ) correlation function

$$g_6(r)/g(r) \sim r^{-1/4} \exp(-r/\xi_6) \quad (14)$$

directly yields the hexatic length scale  $\xi_6$  [54]. In Fig. 8, we show a plot of this hexatic correlation function normalized to the radial distribution function  $g_6(r)/g(r)$ , at a fixed persistence time  $\tau_p$ .

The solid lines are a fit to the OZ prediction Eq. (14) to extract the hexatic length scale  $\xi_6$ . It is clear, at least qualitatively, that  $\xi_6$  tends to increase as the effective temperature  $T_{\text{eff}}$  is lowered. To further illustrate the dependence on the

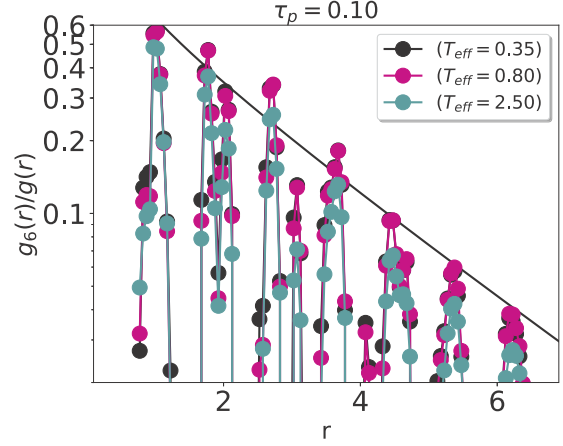


FIG. 8. A plot of  $g_6(r)/g(r)$  at various values of effective temperature but a fixed persistence time  $\tau_p = 0.10$ . Solid lines that indicate a fit to the OZ prediction Eq. (14) are used to extract a hexatic length scale  $\xi_6$ .

persistence time  $\tau_p$ , we show in Fig. 9 a plot of  $\xi_6$  versus  $1/T_{\text{eff}}$  at various values of persistence times. It is evident from this figure that at lower temperatures, the effect  $\tau_p$  on  $\xi_6$  is only marginal. These observations are consistent with our data on local order, shown earlier in Fig. 7. Next, we will discuss another length scale that arises from the microscopic analysis of particle diffusion.

#### D. Diffusion length scale $\sqrt{D\tau_\alpha}$

A microscopic length scale can be constructed from the all particle diffusion coefficient  $D$  and the  $\alpha$ -relaxation time  $\tau_\alpha$  in the form of  $\sqrt{D\tau_\alpha}$  [44]. The realization of this as a growing length scale can be argued from the fact that  $\tau_\alpha$  is a good approximation of the onset time of the Fickian diffusion in typical liquids. The latter clearly becomes larger as the liquid

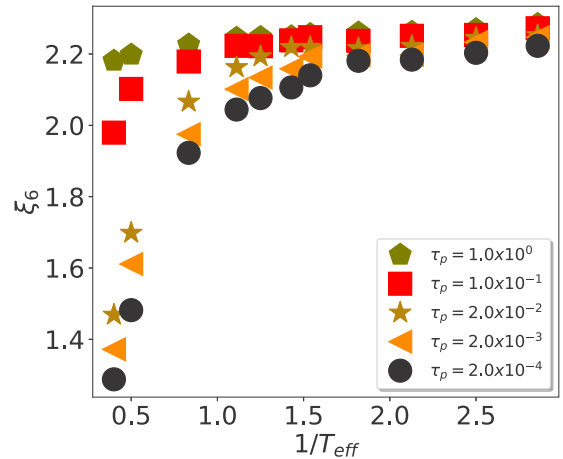


FIG. 9. At lower effective temperatures ( $1/T_{\text{eff}} > 1.0$ ), the hexatic length scale  $\xi_6$  grows very weakly. Moreover, the effect of  $\tau_p$  on  $\xi_6$  at these temperatures is also marginal. Therefore, we are led to the conclusion that  $\xi_6$  is not the dominant length scale that is connected to the growing relaxation time.

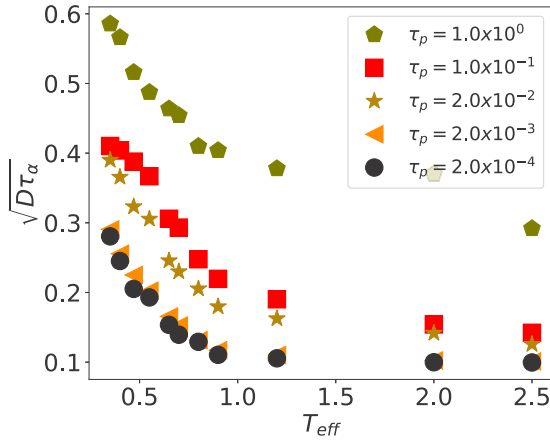


FIG. 10. Length scale ( $\sqrt{D\tau_\alpha}$ ) obtained from the diffusion coefficient increases with the inverse of  $T_{\text{eff}}$  for various persistence times.

is taken to lower temperatures shown in Fig. 10. In Fig. 11, we plot all these length scales as a function of temperature for two different values of persistence times. We further note that in the region of our interest, i.e., at  $T_{\text{eff}} < 1.0$ , the difference between  $D$  and the partial diffusion coefficients of small  $D_S$  and large particles,  $D_L$ , is only marginal (not shown here). We therefore choose  $D$  over these partial diffusivities on the grounds of simplicity. In what follows, we discuss our observations on the dependence of all the length scales reported in this paper, namely  $\xi$ ,  $\xi_6$  and  $\sqrt{D\tau_\alpha}$  as a function of the state parameters,  $\tau_p$  and  $T_{\text{eff}}$ .

#### E. Decoupling of length scales on $T_{\text{eff}}$ and $\tau_p$

It is evident from Fig. 11 that all length scales tend to grow with inverse effective temperature, but the dynamic length scale  $\xi$  clearly dominates all and is therefore clearly decoupled from the others. This is especially true at lower effective temperatures and for all the persistence times considered here. The role of persistence time is to merely push the onset of decoupling toward higher temperatures. One can observe this qualitatively in Fig. 11 where we show our data on all the length scales for two extreme values of  $\tau_p$ , namely 0.0002 (bottom) and 0.1 (top). Similar decoupling of length scales has been studied in volume fraction-dependent studies of passive liquids maintained at a fixed temperature [25].

#### IV. SUMMARY

To summarize our paper, we have performed extensive numerical simulations to extract various length scales near the glass transition in a model active glass forming liquid. The dependence of these length scales on the effective temperatures and persistence times is carefully explored, and a detailed comparison between the dynamic and static length scales is also presented. An important finding of our work is a simple exponential scaling law,  $\tau_\alpha \sim \exp(\mu\xi/T_{\text{eff}})$ , that connects the dynamic length scale  $\xi$  to the concomitant growing time scale  $\tau_\alpha$  through the concept of a chemical potential  $\mu$ —a cost that needs to be scaled in order to form clusters of slow-moving particles. The quantity  $\mu\xi$  then refers to a growing free

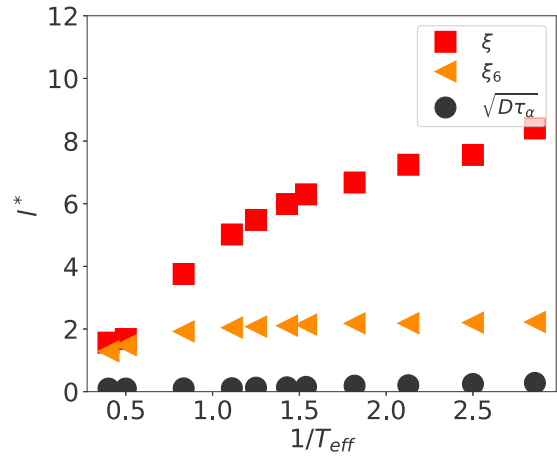
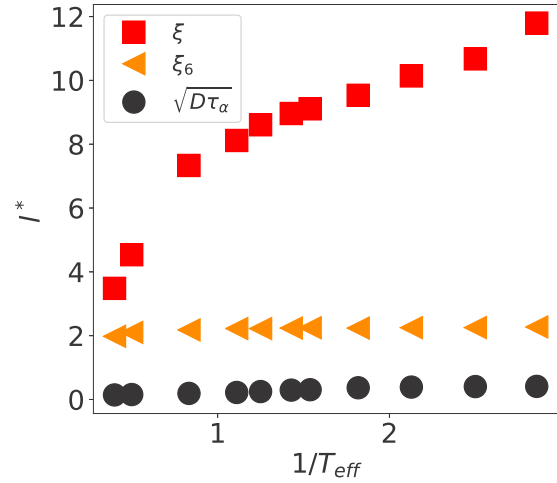


FIG. 11. Length scales vs effective temperature for two different persistence times, namely for  $\tau_p = 0.1$  (top) and  $\tau_p = 0.0002$  (bottom). It is evident that all length scales grow with inverse effective temperature. Note that for any given persistence time, the dynamical length scale  $\xi$  progressively decouples from the other length scales as the effective temperature is lowered. The onset of this decoupling, however, is pushed to higher effective temperatures as the persistence time is increased.

energy barrier that can account for slower rearrangement of the aforementioned clusters, as  $T_{\text{eff}}$  is lowered. Our estimated  $\xi$  also agrees very well with the size of these clusters, further asserting our claim. We also observe that  $\xi$  dominates over the static length scale  $\xi_6$  at all temperatures and persistence times considered here. The latter is saturated at lower temperatures and is only marginally affected by the persistence time in this range. There is therefore no general correspondence between  $\xi_6$  and  $\xi$  in the case of an “athermal” active liquid. The findings reported in our paper are robust over four orders of magnitude variation in persistence time and hence should be of great utility to researchers interested in the glassy dynamics of a generic active liquid.

#### ACKNOWLEDGMENTS

We thank Ethayaraja Mani and Smarajit Karmakar for comments and discussions. All simulations were done on the

VIRGO super cluster of IIT Madras and the HPC-Physics cluster of our group. Support from DST INSPIRE Faculty

Grant 2013/PH-59 and the New Faculty Seed Grant (NFSG), IIT Madras, is gratefully acknowledged.

- 
- [1] M. D. Ediger, *Annu. Rev. Phys. Chem.* **51**, 99 (2000).
- [2] R. Richert, *J. Phys.: Condens. Matter* **14**, R703 (2002).
- [3] C. Donati, S. C. Glotzer, P. H. Poole, W. Kob, and S. J. Plimpton, *Phys. Rev. E* **60**, 3107 (1999).
- [4] L. Berthier, *Phys. Rev. E* **69**, 020201(R) (2004).
- [5] S. Karmakar, C. Dasgupta, and S. Sastry, *Proc. Natl. Acad. Sci. U.S.A.* **106**, 3675 (2009).
- [6] S. C. Glotzer, V. N. Novikov, and T. B. Schröder, *J. Chem. Phys.* **112**, 509 (2000).
- [7] H. C. Andersen, *Proc. Natl. Acad. Sci. U.S.A.* **102**, 6686 (2005).
- [8] T. E. Angelini, E. Hannezo, X. Trepate, M. Marquez, J. J. Fredberg, and D. A. Weitz, *Proc. Natl. Acad. Sci. U.S.A.* **108**, 4714 (2011).
- [9] E.-M. Schoetz, M. Lanio, J. A. Talbot, and M. L. Manning, *J. R. Soc., Interface* **10**, 20130726 (2013).
- [10] N. Gravish, G. Gold, A. Zangwill, M. A. Goodisman, and D. I. Goldman, *Soft Matter* **11**, 6552 (2015).
- [11] N. Lačević, F. W. Starr, T. Schröder, and S. Glotzer, *J. Chem. Phys.* **119**, 7372 (2003).
- [12] S. Whitelam, L. Berthier, and J. P. Garrahan, *Phys. Rev. Lett.* **92**, 185705 (2004).
- [13] R. S. L. Stein and H. C. Andersen, *Phys. Rev. Lett.* **101**, 267802 (2008).
- [14] S. Karmakar, C. Dasgupta, and S. Sastry, *Phys. Rev. Lett.* **105**, 015701 (2010).
- [15] L. Berthier, G. Biroli, J.-P. Bouchaud, L. Cipelletti, D. El Masri, D. L'Hôte, F. Ladieu, and M. Pierno, *Science* **310**, 1797 (2005).
- [16] C. Dalle-Ferrier, C. Thibierge, C. Alba-Simionesco, L. Berthier, G. Biroli, J.-P. Bouchaud, F. Ladieu, D. L'Hôte, and G. Tarjus, *Phys. Rev. E* **76**, 041510 (2007).
- [17] C. Crauste-Thibierge, C. Brun, F. Ladieu, D. L'Hôte, G. Biroli, and J.-P. Bouchaud, *Phys. Rev. Lett.* **104**, 165703 (2010).
- [18] G. Biroli and J.-P. Bouchaud, *Europhys. Lett.* **67**, 21 (2004).
- [19] G. Biroli, J.-P. Bouchaud, K. Miyazaki, and D. R. Reichman, *Phys. Rev. Lett.* **97**, 195701 (2006).
- [20] L. Berthier, G. Biroli, J.-P. Bouchaud, W. Kob, K. Miyazaki, and D. Reichman, *J. Chem. Phys.* **126**, 184503 (2007).
- [21] G. Szamel, *Phys. Rev. Lett.* **101**, 205701 (2008).
- [22] G. Szamel and E. Flenner, *Phys. Rev. E* **81**, 031507 (2010).
- [23] I. Tah, S. Sengupta, S. Sastry, C. Dasgupta, and S. Karmakar, *Phys. Rev. Lett.* **121**, 085703 (2018).
- [24] T. Kawasaki and H. Tanaka, *J. Phys.: Condens. Matter* **22**, 232102 (2010).
- [25] T. Kawasaki and H. Tanaka, *J. Phys.: Condens. Matter* **23**, 194121 (2011).
- [26] T. R. Kirkpatrick, D. Thirumalai, and P. G. Wolynes, *Phys. Rev. A* **40**, 1045 (1989).
- [27] T. R. Kirkpatrick and D. Thirumalai, *Rev. Mod. Phys.* **87**, 183 (2015).
- [28] E. Flenner, G. Szamel, and L. Berthier, *Soft Matter* **12**, 7136 (2016).
- [29] R. Mandal, P. J. Bhuyan, M. Rao, and C. Dasgupta, *Soft Matter* **12**, 6268 (2016).
- [30] R. Mandal, P. J. Bhuyan, P. Chaudhuri, M. Rao, and C. Dasgupta, *Phys. Rev. E* **96**, 042605 (2017).
- [31] F. Giavazzi, M. Paoluzzi, M. Macchi, D. Bi, G. Scita, M. L. Manning, R. Cerbino, and M. C. Marchetti, *Soft Matter* **14**, 3471 (2018).
- [32] Q.-L. Lei, M. P. Ciamarra, and R. Ni, *Sci. Adv.* **5**, eaau7423 (2019).
- [33] É. Fodor, C. Nardini, M. E. Cates, J. Tailleur, P. Visco, and F. van Wijland, *Phys. Rev. Lett.* **117**, 038103 (2016).
- [34] F. Donado, R. Moctezuma, L. López-Flores, M. Medina-Noyola, and J. Arauz-Lara, *Sci. Rep.* **7**, 12614 (2017).
- [35] S. Das, G. Gompper, and R. G. Winkler, *New J. Phys.* **20**, 015001 (2018).
- [36] W. Kob and H. C. Andersen, *Phys. Rev. Lett.* **73**, 1376 (1994).
- [37] W. Kob and H. C. Andersen, *Phys. Rev. E* **51**, 4626 (1995).
- [38] N. D. Mermin and H. Wagner, *Phys. Rev. Lett.* **17**, 1133 (1966).
- [39] N. D. Mermin, *Phys. Rev.* **176**, 250 (1968).
- [40] E. Flenner and G. Szamel, *Nat. Commun.* **6**, 7392 (2015).
- [41] B. Illing, S. Fritschi, H. Kaiser, C. L. Klix, G. Maret, and P. Keim, *Proc. Natl. Acad. Sci. U.S.A.* **114**, 1856 (2017).
- [42] S. Vivek, C. P. Kelleher, P. M. Chaikin, and E. R. Weeks, *Proc. Natl. Acad. Sci. U.S.A.* **114**, 1850 (2017).
- [43] R. Mannella and V. Palleschi, *Phys. Rev. A* **40**, 3381 (1989).
- [44] E. Flenner, M. Zhang, and G. Szamel, *Phys. Rev. E* **83**, 051501 (2011).
- [45] N. Lacević and S. Glotzer, *J. Phys.: Condens. Matter* **15**, S2437 (2003).
- [46] M. Goldstein, *J. Chem. Phys.* **51**, 3728 (1969).
- [47] F. H. Stillinger and T. A. Weber, *Phys. Rev. A* **25**, 978 (1982).
- [48] S. Sastry, P. G. Debenedetti, and F. H. Stillinger, *Nature (London)* **393**, 554 (1998).
- [49] P. G. Debenedetti and F. H. Stillinger, *Nature (London)* **410**, 259 (2001).
- [50] F. Sciortino, *J. Stat. Mech.* (2005) P05015.
- [51] E. Lerner, I. Procaccia, and J. Zylberg, *Phys. Rev. Lett.* **102**, 125701 (2009).
- [52] S. K. Nandi, R. Mandal, P. J. Bhuyan, C. Dasgupta, M. Rao, and N. S. Gov, *Proc. Natl. Acad. Sci. U.S.A.* **115**, 7688 (2018).
- [53] T. Kawasaki, T. Araki, and H. Tanaka, *Phys. Rev. Lett.* **99**, 215701 (2007).
- [54] H. Tanaka, T. Kawasaki, H. Shintani, and K. Watanabe, *Nat. Mater.* **9**, 324 (2010).